

28 **Highlights**

- 29 - Experimental studies on biogenic CaCO₃ dissolution provide novel insights into
30 field sample observations and biomineralization processes
31 - Experimental data aid the interpretation of aberrant coccolith morphology in
32 field samples
33 - In *C. braarudii* partial dissolution reveals a nanostructure in the distal shield
34 - The nanostructure in *C. braarudii* requires adjustments in biomineralization
35 models

36

37 **Abstract**

38 Coccolith dissolution in the water column is an important process in the marine carbon
39 cycle. Identifying dissolution in water column samples has been difficult due to a lack
40 of experimental reference datasets showing dissolution morphologies.~~RC2~~ We
41 conducted a laboratory CaCO₃ dissolution experiment to detect differential dissolution
42 morphologies of three selected coccolithophore (abundant marine calcareous
43 phytoplankton) species, *Coccolithus braarudii*, *Helicosphaera carteri*, and
44 *Scyphosphaera apsteinii*. These species were selected because they are ecologically and
45 biogeochemically important (significant contributors to CaCO₃ production) and have
46 been less studied than *Gephyrocapsa*. Muroliths of *S. apsteinii* dissolve faster than
47 lopadoliths, which in turn dissolve as fast as *H. carteri* but faster than *C. braarudii*. In *S.*
48 *apsteinii* lopadoliths, dissolution rate depends on the crystallographic orientation of the
49 crystals.~~RC2~~ Lopadolith R-units dissolve faster than V-units. Comparison with field
50 samples shows that experimental data are helpful when interpreting field samples. For
51 example, we identify dissolution in water and sediment samples reported in the
52 literature. In *C. braarudii* dissolution reveals a nanostructure on the proximal side of the
53 distal shield, an observation that has implications for coccolith biomineralization
54 models, which do not currently account for the formation of such a structure. This
55 nanostructure features “units” of ca 50-100 nm and resembles the nanostructure well
56 known from extracellular calcifiers such as molluscs and foraminifera. Whether this
57 resemblance is underpinned by a similar formation mechanism remains unknown, but
58 we think this unlikely.~~RC2~~

59

Formatted: Font: Italic

60 **1) Introduction**

61 Present anthropogenic CO₂ concentration changes, both atmospheric and marine,
62 cannot be fully understood without considering marine calcium carbonate, largely
63 produced by calcifying organisms (Broecker and Peng 1982, Morse and Mackenzie
64 1990). These calcifying organisms influence air-sea CO₂ exchange in several ways, e.g.
65 through particulate inorganic- and organic carbon production in the surface ocean but
66 also through export of calcium carbonate to the deep ocean (Morse and Mackenzie
67 1990). The most productive marine calcium carbonate (CaCO₃) producers are pelagic
68 organisms, with coccolithophores contributing ca. 90% of global pelagic CaCO₃
69 production (Ziveri et al., 2023) and ca. 50% of CaCO₃ sedimentation (Milliman 1993,
70 Broecker and Clark 2009). Dissolution of CaCO₃ in the photic zone is an important
71 process in the marine CaCO₃ cycle (Ziveri et al. 2023; Subhas et al. 2022; Sulpis et al.
72 2021). The importance of dissolution for the marine C-cycle has two main aspects.
73 Firstly, dissolution of CaCO₃ releases two moles of alkalinity per one mole of dissolved
74 inorganic carbon, thereby shifting the seawater C-system towards higher pH values
75 (Zeebe and Wolf-Gladrow, 2001). Secondly, the loss of ballast minerals reduces carbon
76 export efficiency thereby influencing the C-cycle long-term (Klaas and Archer
77 2002).~~RC2~~ In addition to occurring in the open ocean photic zone, dissolution of
78 carbonates in general, and coccoliths in particular, may also occur in sediments and
79 coastal CO₂ vent sites (Honjo 1975, Ziveri et al 2014).

Formatted: Subscript

Formatted: Subscript

80 Assessing coccolith dissolution in these diverse settings can be challenging, but partial
81 dissolution morphologies as identified in electron micrographs have proved a useful tool
82 (e.g. Langer et al 2007, Ziveri et al 2014). Knowledge of such differential dissolution
83 morphologies will aid interpretation of field samples, e.g. the degree of dissolution in
84 one species will inform inferences about the degree of dissolution in other species.
85 More fundamentally, knowledge about dissolution morphologies will enable us to
86 accurately distinguish malformation / under-calcification from dissolution, which is not
87 necessarily an easy task (Young 1994). Finally, dissolution might reveal informative
88 structural features (Langer et al 2007). The main goal of our study is to provide a
89 dissolution-morphology reference dataset which can be used to identify dissolution in
90 water column samples. The applicability of our data to sediment samples might be more
91 limited as discussed below.~~RC2~~ The interpretation of field samples is difficult, however,
92 because the degree, and even the mere fact, of dissolution often need to be inferred from

93 the micrographs alone, without precise knowledge of the physico-chemical conditions
94 leading to the observed morphology. For example, in surface sediments *Calcidiscus*
95 *leptoporus* coccoliths (placoliths characterized by two shield-like plates connected by a
96 central tube) lacking proximal shields have been taken as a sign of heavy dissolution
97 (Roth and Berger 1975), which has been proposed as a proxy for dissolution in the
98 sedimentary record (Matsuoka 1999). Only an experimental study could show that
99 separation of the shields is the first observable dissolution feature occurring at less than
100 8% mass loss (Langer et al 2007) revealing the “weak spot” at the proximal end of the
101 tube (the position of the proto-coccolith ring, Young et al 2004).The first task is to
102 distinguish dissolution from malformation and the second task is to assess the degree of
103 dissolution. *Calcidiscus leptoporus* coccoliths (placoliths characterized by two shield-
104 like plates connected by a central tube) lacking proximal shields have been observed in
105 surface sediments, leading to the conclusion that single shields are a sign of heavy
106 dissolution (Roth and Berger 1975), which has been proposed as a proxy for dissolution
107 in the sedimentary record (Matsuoka 1999). Only an experimental study could show
108 that separation of the shields is the first observable dissolution feature occurring at less
109 than 8% mass loss (Langer et al 2007). The latter study, in addition to aiding the
110 interpretation of field samples, revealed structural features unobservable in standard
111 scanning electron microscope (SEM) observations, i.e. the “weak spot” at the proximal
112 end of the tube (the position of the proto-coccolith ring, Young et al 2004) leading to
113 shield separation at the first stages of dissolution.

114 Despite the importance of experimental studies showing graded dissolution of
115 coccoliths, only a few such studies have been conducted (McIntyre & McIntyre 1971,
116 Burns 1977, Kleijne 1990, Henriksen et al 2004, Langer et al 2006b, Holcová and
117 Scheiner 2023), with a focus on *Gephyrocapsa spp.* in particular *G. huxleyi*, a widely
118 used model species (Wheeler et al 2023).Despite the importance of experimental studies
119 showing graded dissolution of coccoliths, only a few such studies have been conducted,
120 with a focus on *Gephyrocapsa spp.* in particular *G. huxleyi*, a widely used model species
121 (McIntyre & McIntyre 1971, Burns 1977, Kleijne 1990, Henriksen et al 2004, Langer et
122 al 2006b, Holcová and Scheiner 2023).The degree of dissolution in *G. huxleyi* water
123 column samples is difficult to assess as there are variations of progressive dissolution
124 patterns with e.g. warm- and cold-water phenotypes (Burns 1977). The latter author
125 pointed out that a tropical *G. huxleyi* loses the central grille in the first stages of

Formatted: Font: Italic

Formatted: Font: Italic

126 dissolution, while a cold-water phenotype does not. Calcite removal from the long
127 margin of the radial elements is a sign of early dissolution in the cold-water phenotype
128 but not in a heavily calcified phenotype. These and similar observations made by Burns
129 (1977) show that assessing the degree of dissolution in *G. huxleyi* is not an easy task
130 and morphotype-specific assessments are required.^{RC2} While *G. huxleyi* is numerically
131 the most abundant coccolithophore in present oceans, its contribution to
132 coccolithophore CaCO₃ production is rivalled by some genera with larger coccoliths,
133 such as *Calcidiscus* and *Coccolithus* (Wheeler et al 2023). The relatively recent
134 appearance of *G. huxleyi* in the fossil record implies that this species is not applicable to
135 deep time sediment core studies (Henderiks et al 2022). It is therefore worthwhile also
136 studying genera with larger coccoliths and mass, biogeographically biogeochemically
137 important (Ziveri et al., 2004), and with a more extensive evolutionary history, e.g.
138 *Coccolithus*, *Helicosphaera*, and *Scyphosphaera* (Henderiks et al 2022). The latter
139 genera are not as abundant as *G. huxleyi* but play an important role in coccolithophore
140 CaCO₃ production and export in modern oceans (Baumann et al., 2004; Daniels et al.,
141 2014, 2016; Gafar et al., 2019; Ziveri et al., 2007).

Formatted: Font: Italic

Formatted: Font: Italic

Formatted: Subscript

142 Based largely on field sediment studies, it is accepted that some coccolith forms
143 dissolve faster than others. While *G. huxleyi* and *Umbilicosphaera sibogae* are among
144 the fast-dissolving placolith bearing species, *G. oceanica*, *C. leptoporus*, and *C.*
145 *pelagicus* are comparatively slow-dissolving (McIntyre & McIntyre 1971, Berger 1973,
146 Roth and Coulbourn 1982). These studies have not assessed how dissolution
147 morphologies of different species relate to each other. In other words, which dissolution
148 morphology of species x corresponds to a given dissolution morphology of species y?
149 ~~Knowledge of such differential dissolution morphologies will aid interpretation of field~~
150 ~~samples, e.g. the degree of dissolution in one species will inform inferences about the~~
151 ~~degree of dissolution in other species. More fundamentally, knowledge about~~
152 ~~dissolution morphologies will enable us to accurately distinguish malformation / under-~~
153 ~~calcification from dissolution, which is not necessarily an easy task (Young 1994).~~
154 ~~Finally, dissolution might reveal informative structural features, as in the *C. leptoporus*~~
155 ~~example given above. We hypothesize that dissolution morphologies will be different~~
156 ~~from malformations (Dianco et al 2025, Langer et al. 2006, Langer et al 2021, Gerecht~~
157 ~~et al 2015, Meyer et al 2020) and therefore a dissolution reference dataset will enable us~~
158 ~~to unambiguously identify dissolution in field samples. The experimental setup chosen~~

159 ~~here is ideally suited to analyse sequential dissolution morphology with nanometric~~
160 ~~resolution. This enables the identification of different dissolution stages in field~~
161 ~~samples, providing additional information over and above the mere distinction of~~
162 ~~dissolution features and malformations.~~

163 Coccoliths contain crystals of different orientations, sizes, and shapes. A typical feature,
164 for example, is the presence of crystals with radial c-axis orientations (R-units) and
165 others with vertical c-axis orientations (V-units, Young et al 1992). It might therefore be
166 hypothesized that different crystals display different structural features, not only on the
167 micrometre but also on the nanometre scale. Some of these features might only be
168 discernible in partially dissolved specimens.

169 In this study we selected laboratory cultures of *Coccolithus braarudii*, *Helicosphaera*
170 *carteri*, and *Scyphosphaera apsteinii*, and performed a dissolution experiment to follow
171 their differential dissolution morphologies by means of sequential sampling for SEM
172 analysis. Here we analyse two important aspects of dissolution. Firstly, the selective
173 dissolution of different species relative to each other. Secondly, the evolution of
174 morphology of a given species with progressive dissolution. RC2 We hypothesize that
175 dissolution morphologies will be different from malformations (Bianco et al 2025,
176 Langer et al. 2006, Langer et al 2021, Gerecht et al 2015, Meyer et al 2020) and
177 therefore a dissolution reference dataset will enable us to unambiguously identify
178 dissolution in field samples. The experimental setup chosen here is ideally suited to
179 analyse sequential dissolution morphology with nanometric resolution. This enables the
180 identification of different dissolution stages in field samples, providing additional
181 information over and above the mere distinction of dissolution features and
182 malformations. RC1

183 Experimental dissolution studies provide a good source of information on the evolution
184 of morphology with dissolution, without confounding factors from field studies such as
185 variance in the primary biomineralization morphology.

187 2) Material and Methods

188 2.1) Culture conditions

189 Clonal cultures of *Coccolithus braarudii* (strain RCC1198), *Scyphosphaera*
190 *apsteinii* (strain RCC3598), and *Helicosphaera carteri* (strain RCC1323) were grown in
191 aged (3 months), sterile-filtered (Stericup-GP Sterile Vacuum Filtration System, 0.22 µm
192 pore size, polyethersulfone membrane, Merck) natural surface seawater sampled in the
193 English Channel off Roscoff, France, enriched with 288 µM nitrate, 18 µM phosphate,
194 and silicate, trace metals, and vitamins as in K/2-I ([https://roscoff-culture-](https://roscoff-culture-collection.org/medium-id/k2-i)
195 [collection.org/medium-id/k2-i](https://roscoff-culture-collection.org/medium-id/k2-i)). All strains were obtained from the Roscoff Culture
196 Collection (<http://www.roscoff-culture-collection.org>).

Field Code Changed

197 Cultures were grown under a 16:8 h light:dark cycle at a light intensity of
198 50 µmol photons m⁻² s⁻¹ in temperature-controlled culture incubators. *Coccolithus*
199 *braarudii* RCC1198 was grown at 15°C, while *Scyphosphaera apsteinii* RCC3598 and
200 *Helicosphaera carteri* RCC1323 were grown at 20°C. Cells were grown in dilute batch
201 cultures, ensuring a quasi-constant seawater carbonate system over the course of
202 exponential growth (Hoffmann et al. 2015). Cell densities were determined by flow
203 cytometry immediately after sampling. Cultures used in the dissolution experiment were
204 initially checked by light and scanning electron microscopy to ensure that coccosphere
205 morphology was normal (as observed in light microscopy) and the percentage of
206 coccolith malformations was below 15% (as determined by SEM analysis, Langer and
207 Bode 2011). The latter is a very low percentage of malformations in cultures (in which
208 values up to 90% have been reported, Langer et al 2006, Langer et al 2013), enabling
209 this study to focus on normal coccoliths and their dissolution morphologies, as opposed
210 to the dissolution features of malformed coccoliths (Langer and Bode 2011, Langer et al
211 2013, Langer et al 2023). We chose not to analyse the dissolution morphology of
212 malformed coccoliths because results are intended to be applicable to field samples, in
213 which the percentage of malformed coccoliths is typically only ca. 2% (Langer et al
214 2006, Langer et al 2013). Analysis of the dissolution morphologies of malformed
215 coccoliths would require a different experimental setup, with cultures displaying high
216 proportions of malformed coccoliths. Such an approach would be interesting in itself,
217 but does not fall within the scope of the present study (Langer et al 2006).

218 2.2) Dissolution experiment

219 To study differential dissolution morphologies accurately, the selected species
220 ~~were combined in a single 2.7L bottle have to be exposed to the same seawater, i.e. be~~
221 ~~present in the same vessel~~ (Holcová and Scheiner 2023), in which case only one calcite

222 saturation state (ω) value can be selected. In pre-experiments we found that
223 *Gephyrocapsa huxleyi* coccoliths dissolved more than 10x faster than coccoliths of
224 *Coccolithus braarudii*, *Helicosphaera carteri*, and *Scyphosphaera apsteinii*, meaning it
225 was not possible to include *G. huxleyi* in our experiment. The three other species, *C.*
226 *braarudii*, *H. carteri*, and *S. apsteinii*, displayed broadly similar dissolution kinetics and
227 were therefore suited for our purpose.

228 To start the dissolution experiment, living cells were transferred into a 2.7L bottle
229 containing culture medium that was acidified using calculated amounts of HCl (3.29M)
230 immediately prior to cell transfer. We used acidification to manipulate ω calcite
231 because it is more representative of dissolution scenarios in the field than changes in Ca
232 concentration. Omega calcite is the saturation state of seawater with respect to calcite,
233 with $\omega < 1$ indicating dissolution and $\omega > 1$ potential crystal growth. This
234 decision is important because the manipulation of ω calcite via acidification is
235 more effective than via Ca concentration decrease (Hassenkam et al 2011). We chose to
236 work with living cells, as opposed to isolated coccoliths for the following reasons.
237 Firstly, we wanted our results to be useful for comparison with various dissolution
238 scenarios such as whole cells in copepod and micro-grazer guts, whole cells in marine
239 snow aggregates, whole cells in ocean acidification-affected corrosive waters. Secondly,
240 we wanted to analyse effects of dissolution on coccospheres, as opposed to only on
241 individual coccoliths. Thirdly, removing coccoliths from cells is not always an easy task
242 and often requires chemical or heat treatment which might alter structural integrity and
243 organic content (Manuela Bordiga, personal communication, 2025). Since this is a pilot
244 study, we wanted to keep the experimental setup as straightforward as possible. Follow
245 up studies should deal with modified setups to explore additional factors influencing
246 dissolution patterns. ~~RC2~~ The culture medium prepared using natural surface seawater
247 sampled off Roscoff, France has a typical dissolved inorganic carbon, DIC, of ca 2000
248 $\mu\text{mol kg}^{-1}$ (Johnson et al 2022). We used this value for DIC and measured pH (NBS) =
249 6.44 to calculate ω calcite = 0.033 using the program CO2SYS (Pierrot et al 2011).
250 The calculated value for ω calcite (0.033) was therefore approximate. However,
251 DIC variability of natural surface seawater sampled off Roscoff, France is low, therefore
252 introducing only a negligible inaccuracy in calculated ω calcite in the context of
253 the present study, i.e. an error of ± 0.005 is expected (Johnson et al 2022). The present
254 study was not designed to analyse dissolution kinetics precisely (such as in Subhas et al

255 2018), meaning an approximate determination of the carbonate system is sufficient. We
256 used a Cyberscan 500 pH meter ([Eutech Instruments, UK](#)) equipped with a Mettler
257 Toledo InLab 413/ID67 electrode to determine pH on the NBS scale.

258 Experimental dissolution over a very short space of time (on the order of seconds as in
259 Yang et al 2021) only allows for comparatively low-resolution light micrographs that
260 would have been insufficient for our purpose. The advantage of a short experiment
261 duration, however, is that DIC uptake and gas exchange with the atmosphere, and
262 therefore carbonate system variability, is negligible. Our dissolution experiment,
263 conducted over a duration of 11 hours, was carried out in the dark at 4°C to ensure that
264 cellular metabolism (including photosynthesis and coccolith production) was severely
265 restricted over the course of the experiment. Cell densities were 711 cells/mL for *C.*
266 *braarudii*, 665 cells/mL for *H. carteri*, and 586 cells/mL for *S. apsteinii*. The resultant
267 low overall cell density of 1963 cells/mL contributed to ensuring a quasi-constant
268 carbonate system over the course of the experiment (Langer et al 2006, Langer and
269 Bode 2011, Hoffmann et al 2015). Physico-chemical conditions over the course of the
270 experiment were additionally homogenized by regular mixing, i.e. keeping the cells in
271 suspension. No aggregation of cells occurred and no sedimentation of cells or coccoliths
272 took place. The pH did rise by ca 0.1 over the course of the experiment, but this
273 corresponds to an increase in omega calcite of only ca. 0.005, i.e. the same magnitude as
274 the minor uncertainty introduced by our choice of DIC value (see above).

275 After the dissolution experiment was completed, cells were transferred into normal
276 culture conditions as specified above. All three species, *C. braarudii*, *H. carteri*, and *S.*
277 *apsteinii*, resumed cell division and coccolith production as confirmed by optical
278 inspection using light microscopy. We did not quantify coccolith morphology in re-
279 calcifying cells, but noted that initially coccoliths seemed to display more
280 malformations than prior to the dissolution experiment. [This assessment is based on an](#)
281 [informal analysis by means of light microscopy; no images were taken.](#)~~RC1~~

282 Multiple (15) sequential samples for detailed morphological analysis were taken over
283 the 11 hour duration of the experiment. Samples for SEM analysis were filtered onto
284 polycarbonate filters (0.8 µm pore-size), dried in a drying cabinet at 50°C for 24 h, then
285 sputter-coated with gold-palladium using a Cressington 108 sputter coater (Cressington
286 Scientific Instruments, Watford, UK). Imaging was performed with a Phenom Pro
287 desktop SEM at the Station Biologique de Roscoff, France, and an EI SEM Zeiss Merlin

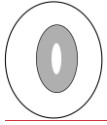
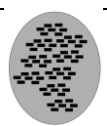
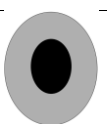
288 at UAB, Barcelona, Spain. All the morphological features described in this study are
 289 discernible using the Phenom Pro desktop SEM. We used the Zeiss Merlin FE-SEM
 290 only to produce images showing the nanostructure on the proximal side of the distal
 291 shield of *C. braarudii* because the latter microscope has a higher resolution. This
 292 nanostructure, however, was discovered using the Phenom Pro desktop SEM.~~RC1~~ An
 293 average of ~350 coccoliths was analysed per sample (Langer and Benner 2009). To
 294 describe dissolution morphologies, we selected conspicuous features that could be
 295 easily followed over the course of the experiment to ensure robust results and to
 296 facilitate application to field samples. In *C. braarudii* and *H. carteri* we analysed
 297 dissolution features of coccospheres in addition to dissolution features of coccoliths. In
 298 *S. apsteinii* only dissolution features of coccoliths were analysed because coccospheres
 299 in this species lack the mechanical stability needed to consistently withstand the
 300 mechanical forces experienced in SEM preparation (Langer et al 2023). The following
 301 morphological features were used to describe dissolution. In *C. braarudii*: 1) etching of
 302 the inner tube, 2) etching of the distal shield, 3) central area bar missing, 4) coccoliths
 303 broken, 5) gaps in coccospheres, 6) coccospheres collapsed, 7) nanostructure visible (on
 304 proximal side of distal shield). In *H. carteri*: 1) etching, 2) coccoliths broken, 3)
 305 coccospheres collapsed. In *S. apsteinii* lopadoliths: 1) etching of base, 2) etching of
 306 barrel, 3) rim serrated, 4) lopadoliths broken, 5) isolated lopadolith V units. In *S.*
 307 *apsteinii* muraliths: 1) centre missing, 2) etching, 3) muraliths broken. Scanning
 308 electron micrographs of all of these features are shown in Figs 1-5. The most important
 309 dissolution features for practical purposes are summarised in Table 1.

310 Table 1. Summary of important dissolution features.

311

Formatted: English (United Kingdom)

<u>coccolith</u>	<u>dissolution</u> <u>feature</u>	<u>sketch</u>
<u><i>C. braarudii</i></u>	<u>etching of</u> <u>inner tube</u>	
<u><i>C. braarudii</i></u>	<u>etching of</u> <u>distal shield</u>	

<u><i>C. braarudii</i></u>	<u>central area</u> <u>bar missing</u>	
<u><i>H. carteri</i></u>	<u>etching</u>	
<u><i>S. apsteinii</i></u> <u>lopadoliths</u>	<u>etching of</u> <u>barrel</u>	
<u><i>S. apsteinii</i></u> <u>lopadoliths</u>	<u>serrated rim</u>	
<u><i>S. apsteinii</i></u> <u>murooliths</u>	<u>etching</u>	
<u><i>S. apsteinii</i></u> <u>murooliths</u>	<u>centre</u> <u>missing</u>	

312

313

314

315 **3) Results and Discussion**

316 *3.1) Differential dissolution: general observations*

317 We subjected living cells of three common coccolithophore species, namely
 318 *Coccolithus braarudii*, *Helicosphaera carteri*, and *Scyphosphaera apsteinii*, to seawater
 319 undersaturated with respect to calcite, i.e. omega calcite ca. 0.033 (see Methods). The
 320 duration of the experiment was 11 hours, at the end of which only a few isolated distal
 321 shield elements of *C. braarudii* remained (Fig 6). Our observation that *C. braarudii* is

322 more dissolution resistant than *H. carteri* tallies well with conclusions drawn from
323 studying Atlantic Ocean floor sediments (Berger 1973). Information on *S. apsteinii* in
324 differential dissolution studies is rare, with this species either only mentioned but not
325 discussed or not mentioned at all (McIntyre & McIntyre 1971, Berger 1973, Roth and
326 Coulbourn 1982). From our data we conclude that *S. apsteinii* lopadoliths display
327 dissolution kinetics similar to *H. carteri*, while *S. apsteinii* muroliths dissolve faster. In
328 *S. apsteinii*, R-units, which are smaller and radially oriented, dissolve conspicuously
329 faster than the larger, vertically oriented V-units (Figs 6, 7, see also Drescher et al
330 2012). Since lopadoliths contain calcite only, as opposed to e.g. aragonite (Walker et al
331 2024), the latter observation illustrates that differential dissolution kinetics of biogenic
332 calcium carbonate cannot be inferred from the polymorph only (Langer and Ziveri
333 2025). *S. apsteinii* lopadolith R-units RC1 conspicuously dissolve faster than V-units
334 RC1 (Figs 6, 7), potentially as a result of the size difference of the individual crystals,
335 with V-units being larger (see also Drescher et al 2012). The different dissolution
336 kinetics of V and R-units in the same lopadolith illustrates that the microstructure of a
337 CaCO₃ biomineral influences dissolution kinetics, which could not be inferred from its
338 polymorph alone (the only polymorph that lopadoliths contain is calcite; Walker et al
339 2024, Langer and Ziveri, in press). Both etching and broken coccoliths appear
340 simultaneously in *S. apsteinii* lopadoliths and *H. carteri* (Figs 6, 7). In *C. braarudii*
341 etching of the inner tube occurs simultaneously with etching in *H. carteri* and *S.*
342 *apsteinii*, but etching of the *C. braarudii* distal shield appears later, possibly because the
343 latter features the largest crystals (Figs 6, 7). Relatively slow dissolution of the distal
344 shield compared to the tube/central area was also observed in *C. leptoporus* and might
345 be a general feature of Coccolithales placoliths (Langer et al 2007).

346 3.2) Comparison with field samples

347 Identification of dissolution in field samples:

348 As noted~~RC1~~As noted in the introduction coccolith dissolution in the water
349 column is being highlighted as a key process, greatly affecting the export production of
350 coccolith CaCO₃ to the bottom sediment. Our experimental results on the sequence of
351 dissolution stages might usefully be applied to study of field samples in order to analyse
352 and track water column dissolution. As a proof of concept we show here (Fig 8) images
353 of *Coccolithus braarudii* and *Helicosphaera carteri* coccoliths from sediment trap
354 samples and of coccoliths from water column samples, in both cases showing

355 dissolution features directly comparable to those we observed experimentally. It is also
356 noteworthy that the nanostructure seen in the experimental samples is visible in the field
357 samples (Fig 8) showing that it is not an experimental artefact. Comparable dissolution
358 features have also been illustrated in the literature, for example by Cubillos et al (2012)
359 and Kleijne (1990), although in some cases they have been ascribed to malformation.

360 It is striking that in the three species studied here dissolution morphologies are clearly
361 different from malformations. The latter do not resemble etching as described here (Figs
362 1-5). This is remarkable considering that it has typically been difficult to distinguish
363 dissolution from malformation, and even fracture, in *G. huxleyi* (McIntyre & McIntyre
364 1971, Burns 1977, Kleijne 1990, Holcová and Scheiner 2023, Young 1994, Langer et al
365 2006b, Langer and Benner 2009, Langer et al 2011). These difficulties in identifying
366 dissolution morphology in *G. huxleyi* are particularly conspicuous in morpho-type B/C,
367 but are clearly noticeable in type A as well (own observations, unpublished). It might be
368 speculated that dissolution is easier to identify in type R because the latter features
369 fused distal shield elements which makes the overall morphology more similar to the
370 one of the species studied here. This conjecture is supported by *G. huxleyi* morphotype-
371 specific dissolution morphologies described in water column samples (Burns 1977). It
372 will be worthwhile studying different *G. huxleyi* morphotypes in greater detail. Species-
373 specific dissolution features such as the serrated rim in *S. apsteinii* lopadoliths are also
374 dissimilar to malformations such as type R (Langer et al 2021, Langer et al 2023). The
375 nanostructure on the proximal side of the distal shield of *C. braarudii* is hardly visible
376 in normal as well as malformed coccoliths, whereas it is clearly visible in partially
377 dissolved coccoliths. In *C. braarudii* a concentric hole sometimes appears in malformed
378 coccoliths (Langer et al 2021). This hole is clearly different from etch pits. A typical
379 feature of more severe malformations in placolith bearing species is the distorted
380 architecture of the shields (Bianco et al 2025, Langer et al 2006, Langer and Benner
381 2009, Langer et al 2011, Langer and Bode 2011, Langer et al 2012, Langer et al 2013,
382 Langer et al 2021, Langer et al 2023, Kottmeier et al 2022, Gerech et al 2015, Milner et
383 al 2016, Johnson et al 2022) which does not occur as a result of dissolution.

384 Do the conditions under which dissolution occurs influence dissolution
385 morphologies?~~RC1~~
386 ~~RC1~~As a caveat we will say that dissolution morphologies might well depend on the
387 conditions under which dissolution occurs. For example, the presence or absence of an

Formatted: Indent: First line: 0 cm

Formatted: Font: Italic

388 organic coating around coccoliths results in slightly different dissolution morphologies
389 as seen in high resolution AFM imaging (Henriksen et al 2004). Since we did not
390 remove the organic coating, our results should be best applicable to water samples (with
391 organic coating) as opposed to sediment samples (in which the organic coating might be
392 degraded). That said, the organic coating of coccoliths can still slow down dissolution
393 after 70Ma in the sediment (Sand et al 2014). Whether dissolution morphologies of
394 these ancient coccoliths would be similar to those of cultured specimens remains to be
395 tested. A good candidate would be *C. pelagicus* because it first appeared in the fossil
396 record more than 60 Ma (Henderiks et al 2022). Another aspect to consider is the way
397 undersaturation is achieved. Dissolution kinetics in low-Ca solutions are different from
398 those in low-pH solutions (Hassenkam et al 2011). It is an open question whether
399 dissolution morphologies would differ too. In addition, pressure-driven undersaturation
400 might be relevant for deep-sea sediment samples. All of these issues are amenable to
401 experimental testing and should be the focus of future studies.

402 3.3) Structural integrity of the coccosphere

403 An interesting difference between *C. leptoporus* (Langer et al 2007) on the one
404 hand and *C. braarudii* / *H. carteri* (this study) on the other hand is the structural
405 integrity of coccospheres under dissolution. The earliest feature of dissolution in *C.*
406 *leptoporus* dissolved at an omega calcite of 0.5, is the separation~~earliest feature of~~
407 ~~dissolution in *C. leptoporus* is the separation~~ of the shields resulting in coccosphere
408 collapse (Langer et al 2007). By contrast, in *C. braarudii* and *H. carteri* the earliest
409 dissolution feature is etching leaving the coccospheres intact. Only when coccoliths
410 break due to more pronounced etching do coccospheres collapse in these species (Fig
411 7). This means that living *C. leptoporus* cells are more vulnerable to dissolution than *C.*
412 *braarudii* / *H. carteri* because all three species need a coccosphere to live (Walker et al
413 2018a, Bianco et al., 2025). While a coccosphere comprised of coccoliths produced by
414 the very cell itself is essential for survival in monospecific cultures of these species,
415 mixed-species coccospheres in natural assemblages indicate that coccosphere integrity
416 can be re-established or modified through incorporation of foreign coccoliths (Johns et
417 al 2023). This might mean that a coccosphere compromised through dissolution or
418 malformation might be repaired by incorporating foreign coccoliths. The protective
419 efficacy of such hybrid coccospheres remains to be tested experimentally. However, the
420 vulnerability sequence described above differs from what would be~~RC1~~ This

421 ~~vulnerability sequence differs from what would be~~ expected based on species specific
422 coccolith solubility as inferred from sediment samples, which do not suggest that *C.*
423 *leptoporus* is more vulnerable than *H. carteri* (Berger 1973). Note that we cannot be
424 entirely sure that *C. leptoporus* coccoliths would break faster than *H. carteri* coccoliths
425 when subjected to the same omega calcite because the *C. leptoporus* experiment was
426 conducted at an omega calcite of 0.5 (Langer et al 2007) as opposed to the ca 0.033
427 used here. Nevertheless, considering the very early appearance of separated shields in
428 *C. leptoporus* (Langer et al 2007) and the comparatively late appearance of broken
429 coccoliths in *H. carteri*, it is highly likely that coccosphere collapse in *C. leptoporus*
430 would occur earlier than in *H. carteri* (at a given omega calcite). Although bulk surface
431 waters in most parts of the global ocean are currently supersaturated with respect to
432 calcite, ongoing ocean acidification drives the calcite saturation state towards
433 undersaturation which will be reached in some areas, e.g. the Southern Ocean, around
434 the year 2100, posing a threat to calcifying organisms including coccolithophores
435 (Langer and Ziveri 2025). Please note that most surface waters will remain
436 supersaturated with respect to calcite, so that our results are most directly relevant to
437 locally undersaturated conditions (e.g. upwelling regions, eddies, sea-ice melt, or pore
438 waters). Regardless of the actual threat posed by corrosive waters to living
439 coccolithophores, the argument we are making here centres on relative vulnerability of
440 different species in case of calcite undersaturation. RC2

441 3.4) *A nanostructure in C. braarudii biomineral*

442 A nanostructure on the proximal side of the distal shield in *C. braarudii* became
443 visible 3 hours into the experiment (Fig. 6). The individual “units” of this nanostructure
444 are ca. 50-100 nm in diameter. The distal side of the distal shield does not show this
445 nanostructure. Differences between the proximal and distal sides of the distal shield
446 have previously been reported (Henriksen et al 2004, Young et al 2004). Whereas the
447 distal side of the distal shield consists of crystallographic a-faces, the proximal side
448 seems to be more profoundly regulated by the cell and does not show crystallographic
449 faces (Young et al 2004). The nanostructure shown here is what was described as
450 “tuberculate surface” by Henriksen et al. (2004). The latter authors conclude that the
451 tubercles are part of the calcite structure. We confirm this conclusion which is illustrated
452 particularly well by a side view of these tubercles (Fig. 3D). We can only speculate what
453 effect this nanostructure might have on the dissolution resistance / susceptibility of the

454 distal shield elements. Considering that the distal shield elements of *C. braarudii* are the
455 only coccolith parts of all three species that are still present at the end of the experiment
456 (Fig. 6), it seems clear that they are comparatively dissolution resistant. Whether this
457 resistance stems from the nanostructure or some other feature remains an open question
458 but it is fair to say that the nanostructure does not make coccolith crystals highly
459 susceptible to dissolution. The importance of micro- and nanostructures in differential
460 dissolution behaviour of various biominerals has been recently highlighted in the
461 context of vulnerability to ocean acidification (Langer and Ziveri 2025). It is
462 conceivable that the nanostructure in *C. braarudii* slows down etching and / or provides
463 structural reinforcement. This scenario would be plausible if the nanostructure was an
464 organo-mineral composite structure as opposed to being composed of calcite only
465 (Walker and Langer 2021).~~RC1~~ A nanostructure of similar size in CaCO₃ biominerals is
466 widespread in extracellular calcifiers, where it is a central indicator of a layered growth
467 mechanism featuring particle accretion which is believed to be non-operative in
468 coccolithophores (Kadan et al 2021, Walker and Langer 2021). It remains, however, an
469 open question whether the nanostructure in *C. braarudii* is similar to that in
470 extracellular calcifiers i.e. whether it is also an organo-mineral composite structure
471 (Walker and Langer 2021). This question is pertinent to coccolithophore
472 biomineralization because an extracellular-like nanostructure in coccoliths would call
473 into question widely held views about crystallization of coccolith crystals (Walker and
474 Langer 2021). However, even if the tuberculate nanostructure in *C. braarudii* should
475 turn out to be extracellular-like, it would still be unclear how it is possible that the distal
476 side of the distal shield is different, i.e. shows crystallographic a-faces and no
477 nanostructure. The standard biomineralization model explaining the nanostructure in
478 extracellular calcifiers cannot account for the difference between the two sides of the
479 distal shield in *C. braarudii*, and neither can the standard model of coccolith
480 biomineralization (Young et al 2004, Walker and Langer 2021). This difference between
481 the proximal and the distal side of the distal shield shows how finely tuned
482 morphogenesis in *C. braarudii* is. We can only speculate how this fine tuning is
483 achieved, but the composition of the organic coating might play a role. The composition
484 of coccolith associated polysaccharides is known to be species specific, but we
485 speculate that it might also be site specific within the coccolith vesicle (Walker et al
486 2018b).

Formatted: Font: Italic

Formatted: Font: Italic

487 **4) Conclusions**

488 In summary, our results show that dissolution experiments complement field studies and
489 contribute to a deeper understanding of both coccolith structure and the ecological
490 impact of seawater undersaturation with respect to calcite. We conclude that

491 1) the most dissolution-resistant species is *C. braarudii*, followed by *H. carteri* and *S.*
492 *apsteinii*;

493 2) structural integrity of the coccosphere under dissolution is highest in *C. braarudii*,
494 followed by *H. carteri* and *S. apsteinii*, with *C. leptoporus* probably showing the
495 weakest coccosphere;

496 3) we identify dissolution in published field data where it was not recognised;

497 4) lopadolith R-units dissolve faster than V-units, illustrating that different
498 microstructures in the same coccolith have different dissolution kinetics despite
499 containing the same mineral;

500 5) the nanostructure in the distal shield of *C. braarudii* points to a fine-tuning in
501 coccolith morphogenesis that is not accounted for by our current model of coccolith
502 biomineralization.

503

504 **Acknowledgements**

505 No acknowledgements at this stage.

506 **Funding:**

507 Generalitat de Catalunya (MERS, 2021 SGR00640), Spanish Ministry of Science and
508 Innovation (CEX2019-000940-M), and BIOCAL project (PID2020-113526RB-I00,
509 Spanish Ministry of Science and Innovation). [DFG project BONITOS 541693727](#).

510 **Competing interests**

511 The authors declare no conflict of interests.

512 **Author contributions**

513 GL: conception, experiments, analysis, writing, IP: experiments, writing, JRY: analysis,
514 field samples, writing, PZ: writing.

515 **Data availability**

516 [The data will be archived at PANGAEA and the DOI will be added in the final](#)
517 [version. Data will be made available at Pangaea database.](#)

518

519 **References**

520 [Baumann, K.-H., Böckel, B., and Frenz, M.: Coccolith contribution to South Atlantic](#)
521 [carbonate sedimentation, in: Coccolithophores, edited by: Thierstein, H. R. and Young,](#)
522 [J. R., Springer Berlin Heidelberg, Berlin, Heidelberg, 367–402,](#)
523 https://doi.org/10.1007/978-3-662-06278-4_14, 2004.

524 Berger WH (1973) Deep-sea carbonates: evidence for a coccolith lysocline. Deep-Sea
525 Res 20:917–921

526 Bianco, S., Bordiga, M., Langer, G., Ziveri, P., Cerino, F., Di Giulio, A., and Lupi, C.
527 (2025) Low sensitivity of a heavily calcified coccolithophore under increasing CO₂: the
528 case study of *Helicosphaera carteri*, Biogeosciences, 22, 1821–1837,
529 <https://doi.org/10.5194/bg-22-1821-2025>.

530 Broecker, W. & Clark, E. Ratio of coccolith CaCO₃ to foraminifera CaCO₃ in late
531 Holocene deep sea sediments. Paleocanogr. 24, PA3205 (2009).

532 Broecker, W. S. & Peng, T.-H. Tracers in the Sea. 690 (Lamont-Doherty Geological
533 Observatory, Columbia University, 1982)

534 Broerse, A.T.C., Ziveri, P., Honjo, S., (2000) Coccolithophore (CaCO₃) flux in the Sea
535 of Okhotsk: seasonality, settling and alteration processes Marine Micropaleontology, 39
536 (1-4): 179-200.

537 Burns, D. A. (1977). Phenotypes and dissolution morphotypes of the genus
538 *Gephyrocapsa* Kamptner and *Emiliana huxleyi* (Lohmann). New Zealand Journal of
539 Geology and Geophysics, 20(1), 143-155.

540 Cubillos, J.C., Henderiks, J., Beaufort, L., Howard, W.R., & Hallegraeff, G.M. (2012).
541 Reconstructing calcification in ancient coccolithophores: Individual coccolith weight
542 and morphology of *Coccolithus pelagicus* (sensu lato). Marine Micropaleontology, 92,
543 29-39.

544 [Daniels, C., Poulton, A., Young, J., Esposito, M., Humphreys, M., Ribas-Ribas, M.,](#)
545 [Tynan, E., and Tyrrell, T.: Species-specific calcite production reveals *Coccolithus*](#)
546 [pelagicus as the key calcifier in the Arctic Ocean, *Mar. Ecol. Prog. Ser.*, 555, 29–47,](#)
547 <https://doi.org/10.3354/meps11820>, 2016.

548 [Daniels, C. J., Sheward, R. M., and Poulton, A. J.: Biogeochemical implications of](#)
549 [comparative growth rates of *Emiliana huxleyi* and *Coccolithus* species,](#)
550 [Biogeosciences](#), 11, 6915–6925, <https://doi.org/10.5194/bg-11-6915-2014>, 2014.

551 Drescher B, Dillaman RM, Taylor AR. (2012) Coccolithogenesis In *Scyphosphaera*
552 *apsteinii* (Pymnesiophyceae). *J Phycol.* 2012 Dec;48(6):1343-61. doi: 10.1111/j.1529-
553 8817.2012.01227.x. Epub 2012 Sep 17. PMID: 27009987.

554 [Gafar, N. A., Eyre, B. D., and Schulz, K. G.: Particulate inorganic to organic carbon](#)
555 [production as a predictor for coccolithophorid sensitivity to ongoing ocean acidification,](#)
556 [Limnol. Oceanogr. Letters](#), 4, 62–70, <https://doi.org/10.1002/lol2.10105>, 2019

557 [Gerecht AC, Supraha L, Edvardsen B, Langer G, Henderiks J. 2015. Phosphorus](#)
558 [availability modifies carbon production in *Coccolithus pelagicus* \(Haptophyta\). *Journal*](#)
559 [of Experimental Marine Biology and Ecology](#) 472: 24–31.

560 Gupta, .M., Banerjee, R. & Mergulhao, L. On the nature of the calcareous substrate of
561 a ferromanganese crust from the Vityaz Fracture Zone, Central Indian Ridge: (2002).
562 inferences on paleoceanography. *Geo-Mar Lett* 22, 12–18 (2002).
563 <https://doi.org/10.1007/s00367-002-0091-0>

564 Hassenkam, T., Johnsson, A. M. S., Bechgaard, K., & Stipp, S. L. S. (2011). Tracking
565 single coccolith dissolution with picogram resolution and implications for CO₂
566 sequestration and ocean acidification. *Proceedings of the National Academy of Sciences*
567 of the United States of America, 108, 8571-8576.

568 [Henderiks, J., Sturm, D., Šupraha, L., & Langer, G. \(2022\). Evolutionary Rates in the](#)
569 [Haptophyta: Exploring Molecular and Phenotypic Diversity. *Journal of Marine Science*](#)
570 [and Engineering](#), 10(6), 798. <https://doi.org/10.3390/jmse10060798>

571 Henriksen, K., Young, J. R., Bown, P. R., & Stipp, S. L. S. (2004). Coccolith
572 biomineralisation studied with atomic force microscopy. *Palaeontology*, 47(3), 725-743.

Formatted: German (Germany)

Formatted: German (Germany)

Field Code Changed

573 Hoffmann, R., Kirchlechner, C., Langer, G., Wochnik, A. S., Griesshaber, E., Schmahl,
574 W. W., and Scheu, C. (2015) Insight into *Emiliana huxleyi* coccospheres by focused ion
575 beam sectioning, *Biogeosciences*, 12, 825–834, <https://doi.org/10.5194/bg-12-825-2015>,
576 2015.

577 Holcová K, Scheiner F. (2023). An experimental study on post-mortem dissolution and
578 overgrowth processes affecting coccolith assemblages: A rapid and complex process.
579 *Geobiology*. 2023 Mar;21(2):193-209. doi: 10.1111/gbi.12528. Epub 2022 Oct 11.
580 PMID: 36218003.

581 Honjo, S. 1975. "DISSOLUTION OF SUSPENDED COCCOLITHS IN THE DEEP-
582 SEA WATER COLUMN AND SEDIMENTATION OF COCCOLITH OOZE",
583 *Dissolution of Deep-sea Carbonates*, William V. Sliter, Allan W. H. Bé, Wolfgang H.
584 Berger

585 [Johns, CT et al. Adsorptive exchange of coccolith biominerals facilitates viral infection.](#)
586 [Sci. Adv.9, eadc8728\(2023\). DOI:10.1126/sciadv.adc8728](#)

587 Johnson, R., Langer, G., Rossi, S., Probert, I., Mammone, M., & Ziveri, P. (2022).
588 Nutritional response of a coccolithophore to changing pH and temperature. *Limnology*
589 *and Oceanography*, 67(10), 2309-2324.

590 Kadan Y, Tollervey F, Varsano N, Mahamid J, Gal A. (2021) Intracellular nanoscale
591 architecture as a master regulator of calcium carbonate crystallization in marine
592 microalgae. *Proc Natl Acad Sci U S A*. 2021 Nov 16;118(46):e2025670118. doi:
593 10.1073/pnas.2025670118. PMID: 34772804; PMCID: PMC8694050.

594 Kleijne, A. (1990). Distribution and malformation of extant calcareous nannoplankton
595 in the Indonesian Seas. *Marine Micropaleontology*, 16(3-4), 293-316.

596 Langer, G. & Benner, I. (2009) Effect of elevated nitrate concentration on calcification
597 in *Emiliana huxleyi*. *J. Nannoplankton Res.* 30: 77–80.

598 Langer, G., & Bode, M. (2011). CO2 mediation of adverse effects of seawater
599 acidification in *Calcidiscus leptoporus*. *Geochemistry, Geophysics, Geosystems*, 12(5).
600 <https://doi.org/10.1029/2010GC003393>

Formatted: German (Germany)

Formatted: German (Germany)

Formatted: German (Germany)

Field Code Changed

601 Langer, G., Geisen, M., Baumann, K. H., Kläs, J., Riebesell, U., Thoms, S., & Young, J.
602 R. (2006). Species-specific responses of calcifying algae to changing seawater
603 carbonate chemistry. *Geochemistry, geophysics, geosystems*, 7(9).

Formatted: German (Germany)

604 Langer, G., Gussone, N., Nehrke, G., Riebesell, U., Eisenhauer, A., Kuhnert, H., Rost,
605 B., Trimborn, S., & Thoms, S. (2006b). Coccolith strontium to calcium ratios in
606 *Emiliana huxleyi*: The dependence on seawater strontium and calcium concentrations.
607 *Limnology and Oceanography*, 51(1 I), 310-320.
608 <https://doi.org/10.4319/lo.2006.51.1.0310>

609 Langer, G., Nehrke, G., & Jansen, S. (2007). Dissolution of *Calcidiscus leptopus*
610 coccoliths in copepod guts? A morphological study. *Marine Ecology Progress Series*,
611 331, 139-146.

612 [Langer, G., Oetjen, K., Brenneis, T. \(2013\). On culture artefacts in coccolith
613 morphology. *Helgoland Marine Research*, 67\(2\), 359-369.
614 <https://doi.org/10.1007/s10152-012-0328-x>](#)

Formatted: German (Germany)

615 [Langer G, Taylor AR, Walker CE, Meyer EM, Ben Joseph O, Gal A, Harper GM,
616 Probert I, Brownlee C, Wheeler GL. Role of silicon in the development of complex
617 crystal shapes in coccolithophores. *New Phytol*. 2021 Sep;231\(5\):1845-1857. doi:
618 \[10.1111/nph.17230\]\(https://doi.org/10.1111/nph.17230\). Epub 2021 Mar 9. PMID: 33483994.](#)

619 Langer G, Probert I, Cox MB, Taylor A, Harper GM, Brownlee C, Wheeler G. (2023)
620 The Effect of cytoskeleton inhibitors on coccolith morphology in *Coccolithus braarudii*
621 and *Scyphosphaera apsteinii*. *J Phycol*. 2023 Feb;59(1):87-96. doi: 10.1111/jpy.13303.
622 Epub 2022 Dec 24. PMID: 36380706.

623 [Langer G. & Ziveri P. \(2025\) Vulnerability to ocean acidification of marine calcifying
624 organisms cannot be predicted from the mineral type in their shells. *Limnology and
625 Oceanography Letters* 10\(4\): 448-452. <https://doi.org/10.1002/lo12.70020>](#)

626 Matsuoka, H. (1990) A new method to evaluate dissolution of CaCO₃ in the deep-sea
627 sediments. *Trans. Proc. Paleont. Soc. Jpn.*, 157, 430-434

628 McIntyre A, McIntyre R (1971) Coccolith concentration and differential solution in
629 oceanic sediments. In: Funnel BM, Riedel WR (eds) *The micropaleontology of oceans*.
630 Cambridge University Press, Cambridge, p 253–2610

631 [Meyer, Erin M., Langer, Gerald, Brownlee, Colin, Wheeler, Glen L. and Taylor, Alison](#)
632 [R. 2020 Sr in coccoliths of *Scyphosphaera apsteinii*: Partitioning behavior and role in](#)
633 [coccolith morphogenesis. *Geochimica et Cosmochimica Acta*, 285, 41-54.](#)
634 [10.1016/j.gca.2020.06.023](#)

635 Milliman, J. D. Production and accumulation of calcium carbonate in the ocean: budget
636 of a nonsteady state. *Glob. Biogeochemical Cycles* 7, 927–957 (1993).

637 Morse, J. W. & Mackenzie, F. T. *Geochemistry of sedimentary carbonates*. (Elsevier,
638 1990).

639 Pierrot, D., D. Wallace, E. Lewis, R. Wallace, and W. Wallace. (2011) MS Excel
640 Program Developed for CO₂ System Calculations. ORNL Environmental Sciences
641 Division. doi:10.3334/CDIAC/otg

642 Roth PH, Berger WH (1975) Distribution and dissolution of coccoliths in the south and
643 central Pacific. In: Sliter WV, Be AWH, Berger WH (eds) CaCO₃ dissolution in the
644 deep sea. Cushman Foundation for Foraminiferal Research, Santa Barbara, CA, p 87–
645 113

646 Roth, P. H., & Coulbourn, W. T. (1982). Floral and solution patterns of coccoliths in
647 surface sediments of the North Pacific. *Marine Micropaleontology*, 7(1), 1–52.
648 doi:10.1016/0377-8398(82)90014-7

649 Sand, K., Pedersen, C., Sjoberg, S., Nielsen, J., Makovicky, E., and Stipp, S. (2014).
650 Biomineralization: long-term effectiveness of polysaccharides on the growth and
651 dissolution of calcite. *Cryst. Growth Des.* 14, 5486–5494. doi: 10.1021/cg5006743

652 Subhas, A. V., Rollins, N. E., Berelson, W. M., Erez, J., Ziveri, P., Langer, G., & Adkins,
653 J. F. (2018). The dissolution behavior of biogenic calcites in seawater and a possible
654 role for magnesium and organic carbon. *Marine Chemistry*, 205, 100-112.
655 <https://doi.org/10.1016/j.marchem.2018.08.001>

656 Subhas, A. V., Dong, S., Naviaux, J. D., Rollins, N. E., Ziveri, P., Gray, W., Rae, J. W.
657 B., Liu, X., Byrne, R. H., Chen, S., Moore, C., Martell-Bonet, L., Steiner, Z., Antler, G.,
658 Hu, H., Lunstrum, A., Hou, Y., Kemnitz, N., Stutsman, J., ... Adkins, J. F. (2022).
659 Shallow Calcium Carbonate Cycling in the North Pacific Ocean. *Global*
660 *Biogeochemical Cycles*, 36(5). <https://doi.org/10.1029/2022GB007388>

Formatted: German (Germany)

661 Sulpis, O., Jeansson, E., Dinauer, A., Lauvset, S. K., & Middelburg, J. J. (2021).
662 Calcium carbonate dissolution patterns in the ocean. *Nature Geoscience*, 14(6), 423–
663 428. <https://doi.org/10.1038/s41561-021-00743-y>

664 Walker JM, Langer G. (2021) Coccolith crystals: Pure calcite or organic-mineral
665 composite structures? *Acta Biomater.* 2021 Apr 15;125:83-89. doi:
666 10.1016/j.actbio.2021.02.025. Epub 2021 Feb 22. PMID: 33631395.

667 Walker JM, Greene HJM, Moazzam Y, Quinn PD, Parker JE, Langer G. (2024) An
668 uneven distribution of strontium in the coccolithophore *Scyphosphaera apsteinii*
669 revealed by nanoscale X-ray fluorescence tomography. *Environ Sci Process Impacts.*
670 2024 Jun 19;26(6):966-974. doi: 10.1039/d3em00509g. PMID: 38354057.

671 Walker CE, Taylor AR, Langer G, Durak GM, Heath S, Probert I, Tyrrell T, Brownlee
672 C, Wheeler GL. (2018a) The requirement for calcification differs between ecologically
673 important coccolithophore species. *New Phytol.* 2018 Oct;220(1):147-162. doi:
674 10.1111/nph.15272. Epub 2018 Jun 19. PMID: 29916209; PMCID: PMC6175242.

675 Walker, Charlotte E., Heath, Sarah, Salmon, Deborah L., Smirnoff, Nicholas, Langer,
676 Gerald, Taylor, Alison R., Brownlee, Colin and Wheeler, Glen L. (2018b) An
677 extracellular polysaccharide-rich organic layer contributes to organization of the
678 coccosphere in coccolithophores. *Frontiers in Marine Science*, 5 (AUG), [306].
679 (doi:10.3389/fmars.2018.00306).

680 Wheeler GL, Sturm D, Langer G. (2023) *Gephyrocapsa huxleyi* (*Emiliana huxleyi*) as a
681 model system for coccolithophore biology. *J Phycol.* 2023 Dec;59(6):1123-1129. doi:
682 10.1111/jpy.13404. Epub 2023 Nov 20. PMID: 37983837.

683 Yang M, Batchelor-McAuley C, Barton S, Rickaby REM, Bouman HA, Compton RG.
684 (2021) Opto-Electrochemical Dissolution Reveals Coccolith Calcium Carbonate
685 Content. *Angew Chem Int Ed Engl.* 2021 Sep 13;60(38):20999-21006. doi:
686 10.1002/anie.202108435. Epub 2021 Aug 15. PMID: 34288323; PMCID:
687 PMC8518593.

688 Young, J. R. (1994). Variation in *Emiliana huxleyi* coccolith morphology in samples
689 from the Norwegian EHUX experiment, 1992. *Sarsia*. 79(4): 417-425.

690 Young, J. R. (2008). *Scyphosphaera porosa* Kamptner 1967 rediscovered in the
691 plankton. *Journal of Nanoplankton Research*. 30(1): 35-38

Field Code Changed

692 Young, J. R., Henriksen, K., & Probert, I. (2004). Structure and morphogenesis of the
693 coccoliths of the CODENET species. In Coccolithophores: From molecular processes to
694 global impact, Thierstein, H. R., & Young, J. R. (Eds.), Springer, 191-216.

695 Ziveri, P., Baumann, K.H., Böckel, B. Bollmann, J. and Young, J. (2004) Present day
696 coccolithophore-biogeography in the Atlantic Ocean in Thierstein, H. and Young, J.
697 Eds. Coccolithophores: From Molecular Processes to Global Impact. Springer Verlag:
698 403-428.

699 [Ziveri, P., De Bernardi, B., Baumann, K.-H., Stoll, H. M., and Mortyn, P. G.: Sinking of
700 coccolith carbonate and potential contribution to organic carbon ballasting in the deep
701 ocean, Deep-Sea Res. Pt. II, 54, 659–675, <https://doi.org/10.1016/j.dsr2.2007.01.006>,
702 2007.](#)

703 Ziveri, P., Gray, W. R., Anglada-Ortiz, G., Manno, C., Grelaud, M., Incarbona, A., Rae,
704 J. W. B., Subhas, A. V., Pallacks, S., White, A., Adkins, J. F., & Berelson, W. (2023).
705 Pelagic calcium carbonate production and shallow dissolution in the North Pacific
706 Ocean. Nature Communications, 14(1), 805. <https://doi.org/10.1038/s41467-023-36177->
707 [w](https://doi.org/10.1038/s41467-023-36177-w)

708 Ziveri, P., Passaro, M., Incarbona, A., Milazzo, M., Rodolfo-Metalpa, R., & Hall-
709 Spencer, J. M. (2014). Decline in Coccolithophore Diversity and Impact on Coccolith
710 Morphogenesis Along a Natural CO₂ Gradient. The Biological Bulletin, 226(3), 282–
711 290. <https://doi.org/10.1086/BBLv226n3p282>

712

713 **Figure captions**

714 **Fig 1 *Coccolithus braarudii***

715 **A) coccosphere at t0, no dissolution B) coccosphere; etching of tube and distal shield**
716 **and central area bar missing C) broken coccoliths, etching of tube, central bar missing**
717 **and gaps in coccosphere D) collapsed coccosphere, also showing etching of tube and**
718 **distal shield and central area bar missing E) coccolith, etching of tube and distal shield,**
719 **and central area missing. Note that the etching consistently occurs by opening of sutures**
720 **between elements rather than by dissolution of element surfaces.**

721

722 *Fig 2 Coccolithus braarudii*

723 A) broken coccolith distal shield in distal view. B) broken coccolith proximal view of
724 distal shield showing nanostructure; the arrow indicates isolated distal shield elements
725 in distal view, from another coccolith, not displaying nanostructure on distal and vertical
726 surfaces.

727

728 *Fig 3 Coccolithus braarudii*

729 A) broken coccolith distal shield in proximal view showing nanostructure B) proximal
730 view of distal shield elements showing nanostructure C) proximal view of distal shield
731 elements showing nanostructure; individual "tubercles" of the nanostructure are ca 50-
732 100nm D) isolated distal shield elements showing nanostructure "tubercles" in vertical
733 side view (arrow)

734

735 *Fig 4 Helicosphaera carteri*

736 A) coccosphere at t₀, no dissolution B) coccosphere displaying coccoliths with severe
737 etching and a broken coccolith C) collapsed coccosphere including broken coccoliths D)
738 coccoliths in distal view with etching in flange and blanket E) coccolith in distal view
739 with etching in flange and blanket F) coccolith in proximal view with etching in flange

740

741 *Fig 5 Scyphosphaera apsteinii*

742 A) coccosphere at t₀, no dissolution B) lopadolith base etching (left); muralith centre
743 missing (right) C) lopadolith barrel etching and serrated rim D and E) broken
744 lopadoliths F) isolated V units G) muralith at t₀, no dissolution H) muralith with
745 etching I) lopadolith in distal view showing R- and V units (arrows, Young 2008); and
746 broken muralith (right)

747

748 *Fig 6* Timelines of dissolution. Bars indicate the period during which the respective
749 feature can be observed. For example images of each feature see Figs 1-5.

750

751 Fig 7 Quantification of the observations illustrated in Fig 6. Plotted is the percentage of
752 each analysed feature versus time in hours from start of experiment. A) *Scyphosphaera*
753 *apsteinii* lopadoliths B) *Scyphosphaera apsteinii* muraliths C) *Helicosphaera carteri* D)
754 *Coecolithus braarudii*

755

756 Fig 8 Field samples showing etching patterns comparable to those seen in the
757 experimental samples. All scale bars 2 μm .

758 *Coecolithus braarudii*: A) Lower surface of a broken piece of distal shield showing
759 nanostructure. B) Central area of distal shield showing early stage dissolution. C) Proximal
760 surface showing advanced dissolution.

761 *Helicosphaera carteri*: D) Distal Surface showing early stage dissolution. E) Proximal surface
762 showing advanced dissolution.

763

Fig 1

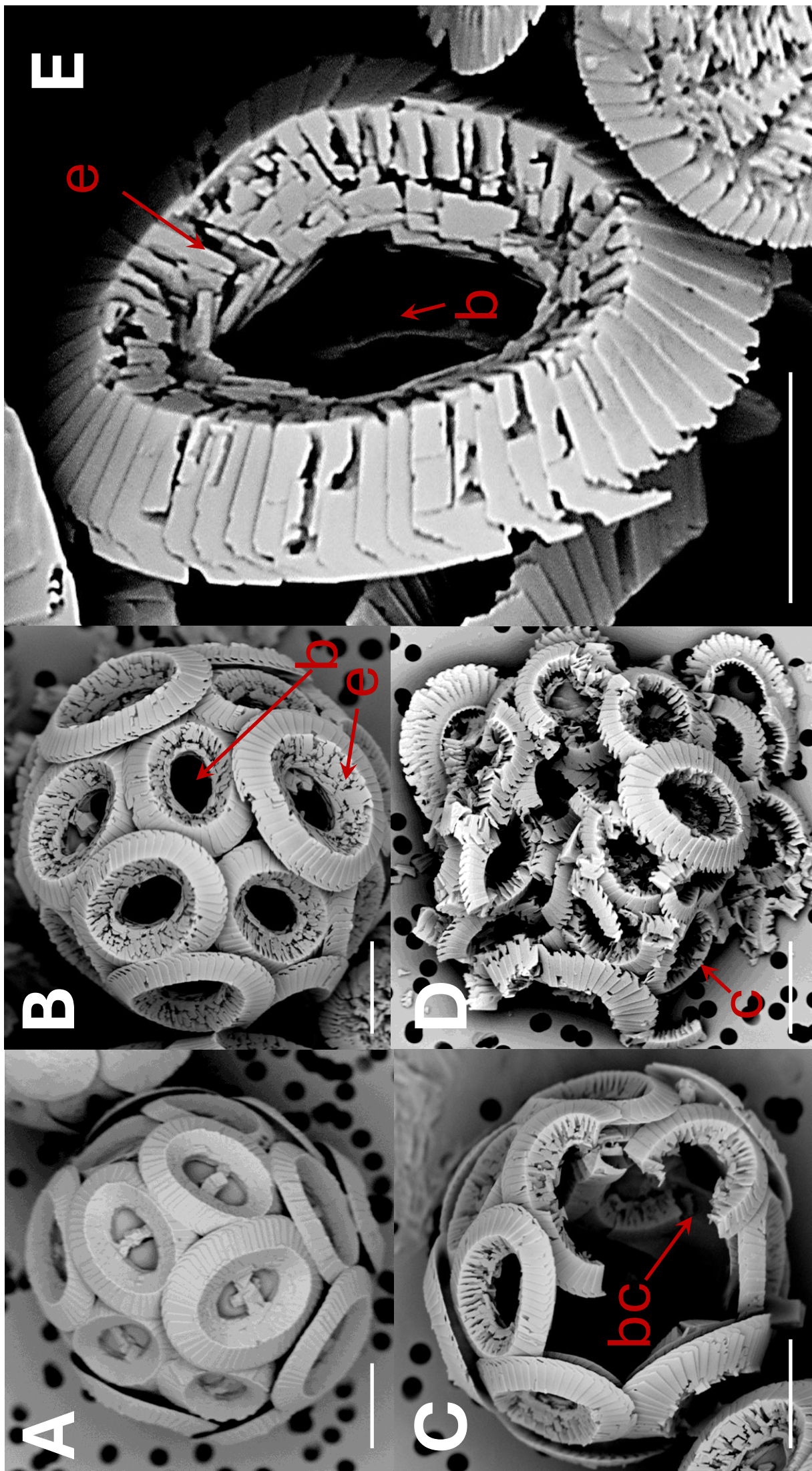


Fig 1 *Coccolithus braarudii*

A) coccosphere at t_0 , no dissolution. Scale bar $5\mu\text{m}$. B) coccosphere; etching (e) of tube and distal shield and central area bar missing (b). Scale bar $5\mu\text{m}$. C) broken coccoliths (bc), etching of tube, central bar missing and gaps in coccosphere. Scale bar $5\mu\text{m}$. D) collapsed coccosphere (c), also showing etching (e) of tube and distal shield and central area bar missing (b). Scale bar $5\mu\text{m}$. E) coccolith, etching (e) of tube and distal shield, and central area bar missing (b). Note that the etching consistently occurs by opening of sutures between elements rather than by dissolution of element surfaces. Scale bar $3\mu\text{m}$.

Fig 2

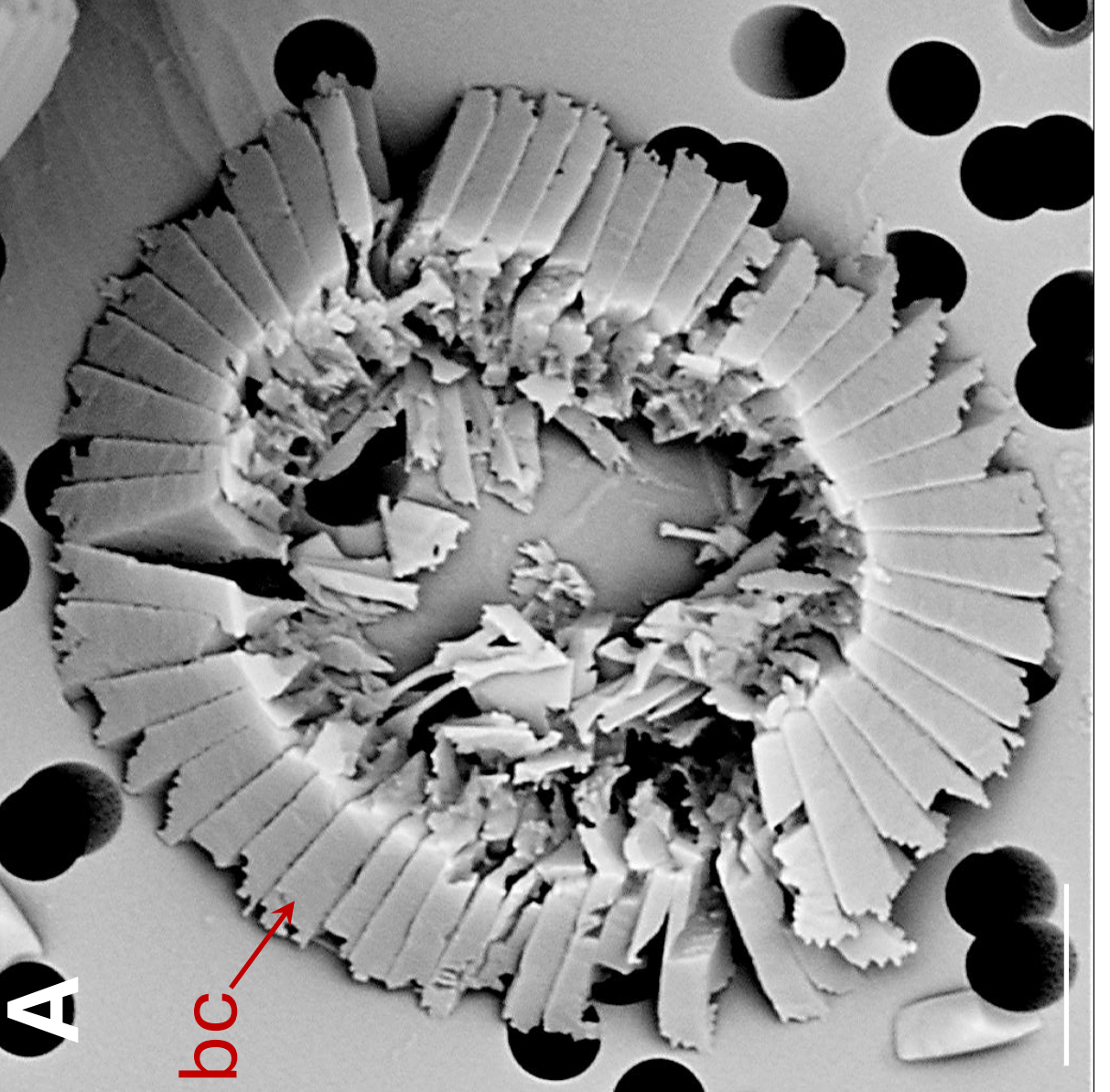
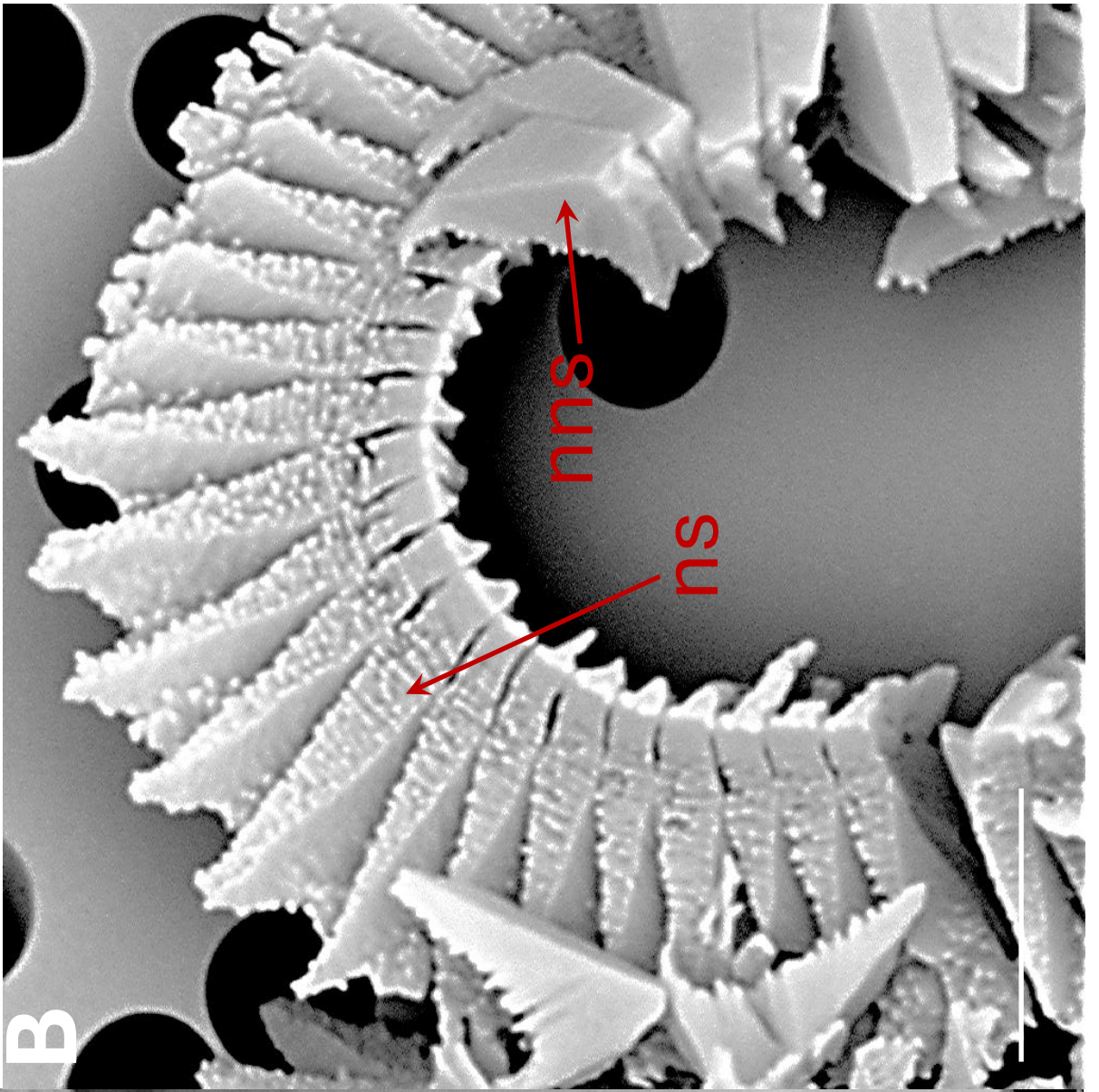


Fig 2 *Coccolithus braarudii*

A) broken coccolith (bc) distal shield in distal view. B) broken coccolith proximal view of distal shield showing nanostructure (ns); the arrow indicates isolated distal shield elements in distal view, from another coccolith, not displaying nanostructure (nns) on distal and vertical surfaces. All scale bars 2 μ m.

Fig 3

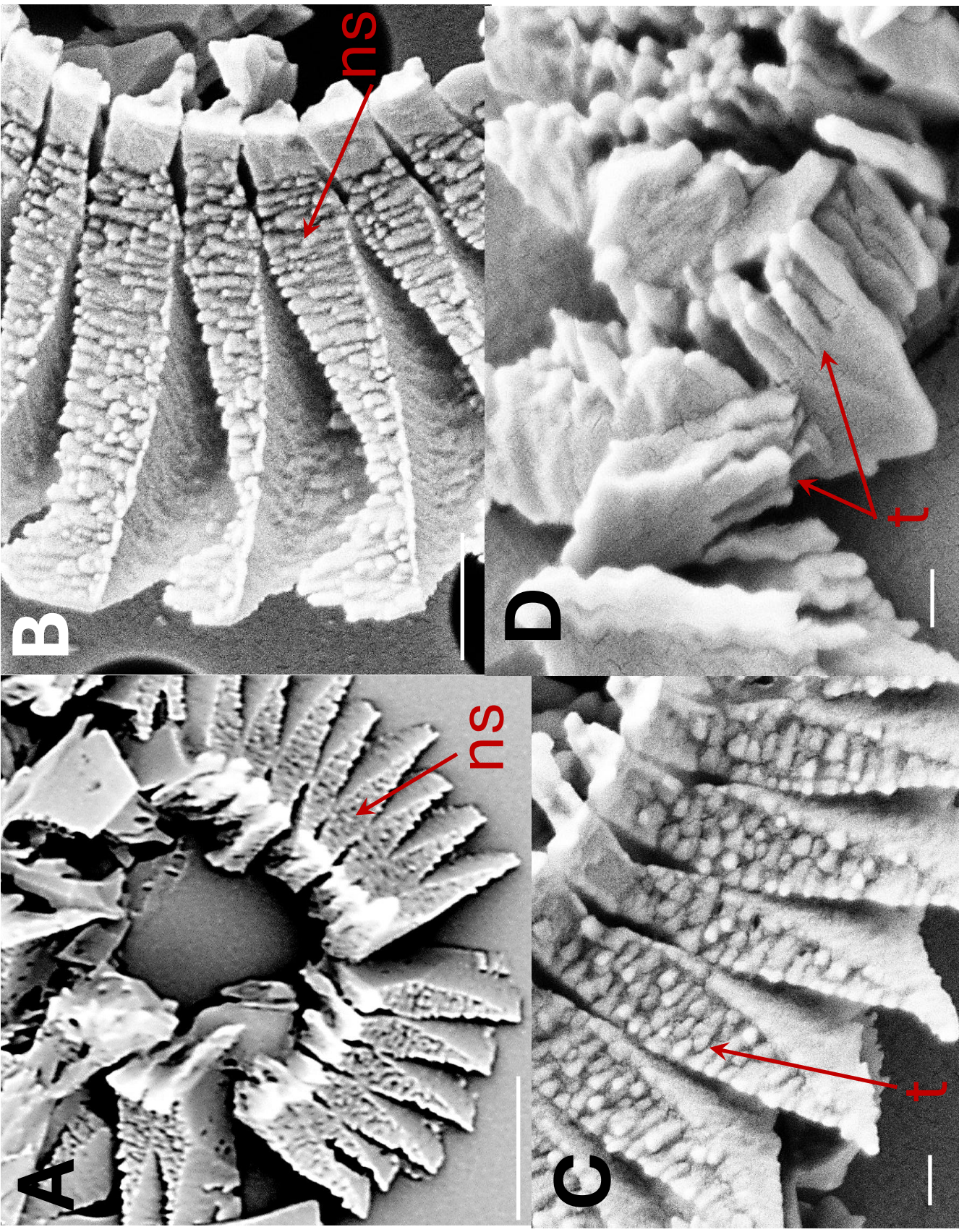


Fig 3 *Coccolithus braarudii*

A) broken coccolith distal shield in proximal view showing nanostructure (ns). Scale bar 2 μ m B) proximal view of distal shield elements showing nanostructure (ns). Scale bar 500nm. C) proximal view of distal shield elements showing nanostructure (ns); individual "tubercles" (t) of the nanostructure are ca 50-100nm, Scale bar 200nm. D) isolated distal shield elements showing nanostructure "tubercles" (t) in vertical side view (arrow). Scale bar 200nm.

Fig 4

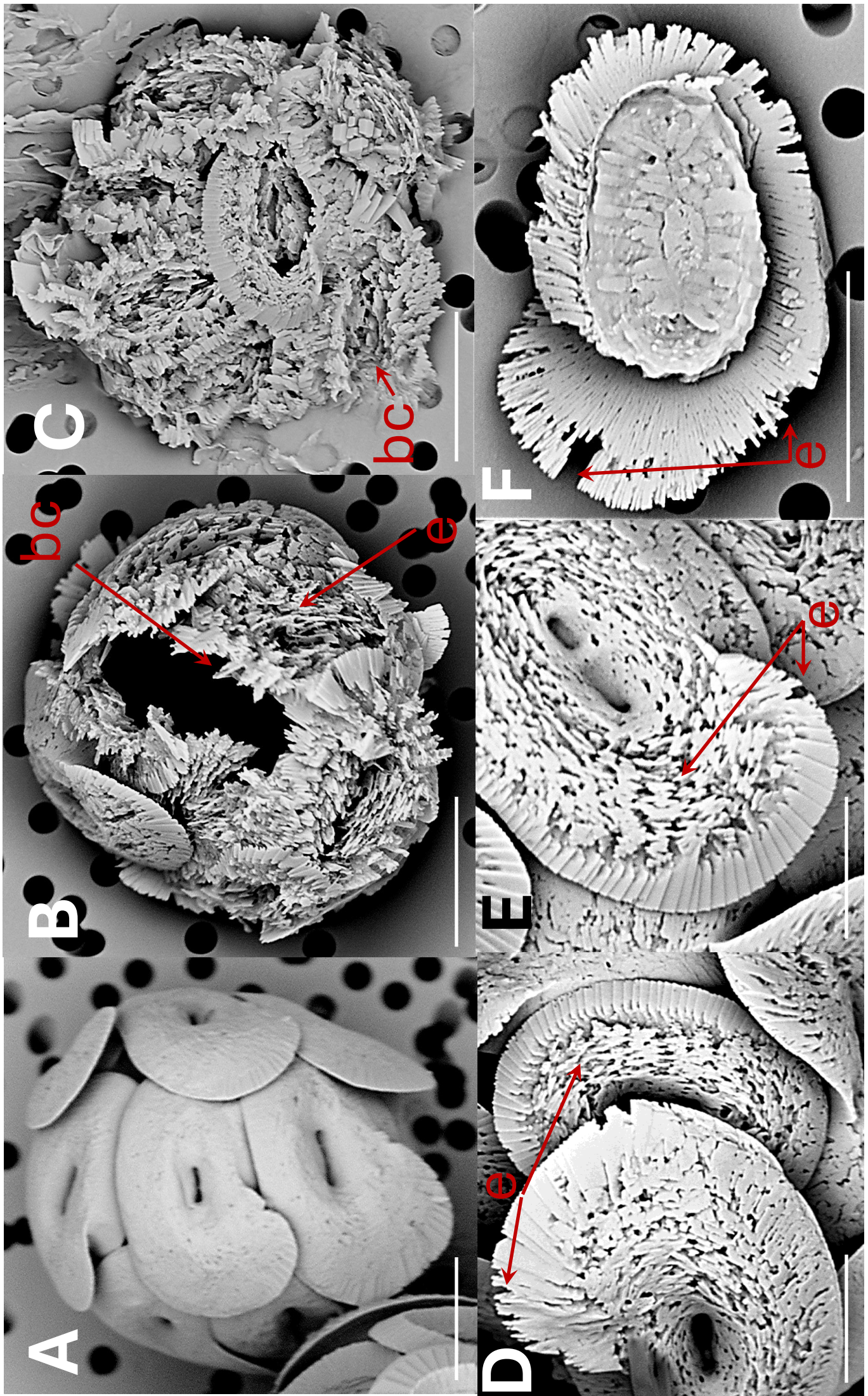


Fig 4 *Helicosphaera carteri*

A) coccosphere at t0, no dissolution. Scale bar 5 μ m. B) coccosphere displaying coccoliths with severe etching (e) and a broken coccolith (bc). Scale bar 5 μ m. C) collapsed coccosphere including broken coccoliths (bc). Scale bar 5 μ m. D) coccoliths in distal view with etching (e) in flange and blanket. Scale bar 3 μ m. E) coccolith in distal view with etching in flange and blanket. Scale bar 2 μ m. F) coccolith in proximal view with etching (e) in flange. Scale bar 5 μ m.

Fig 5

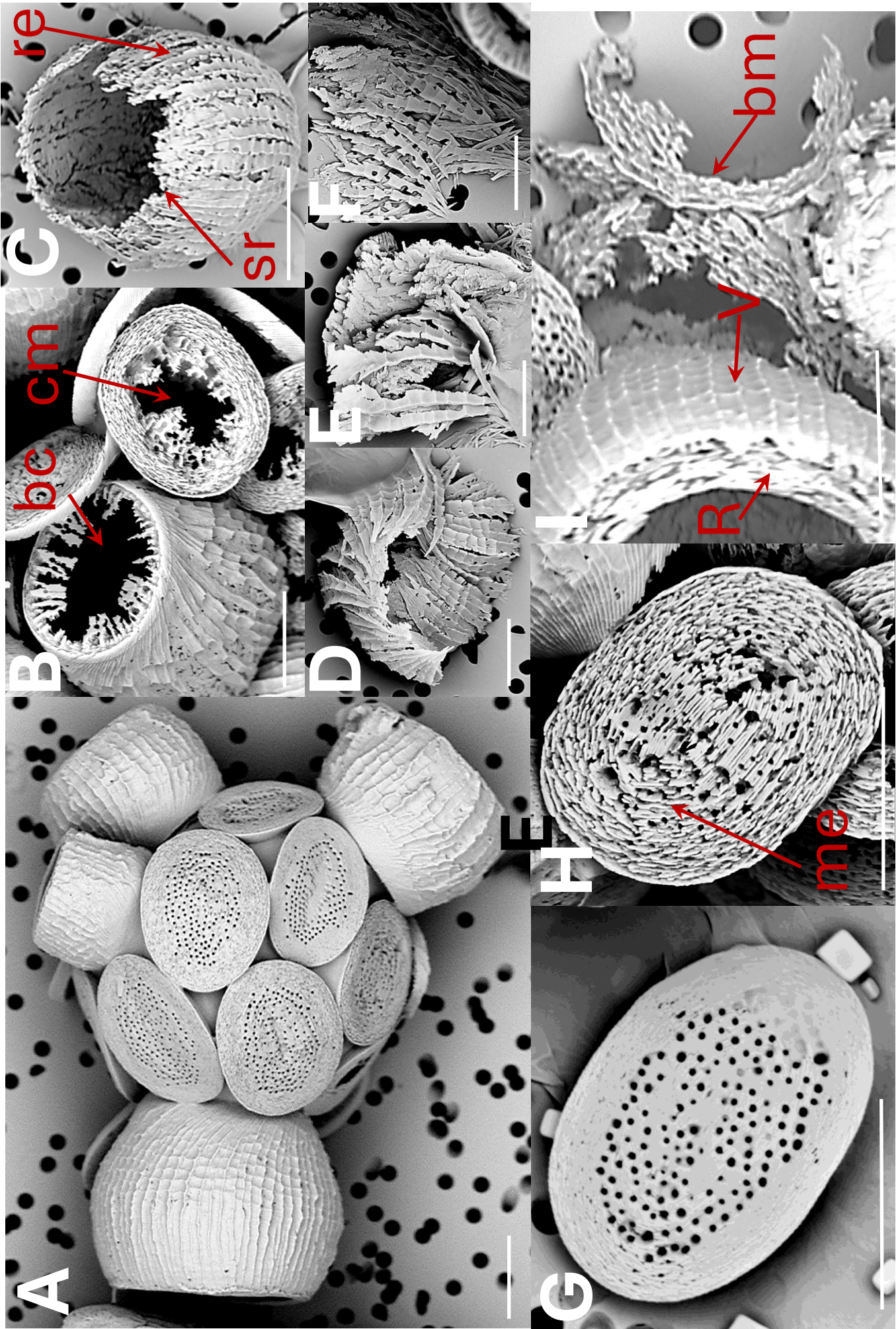
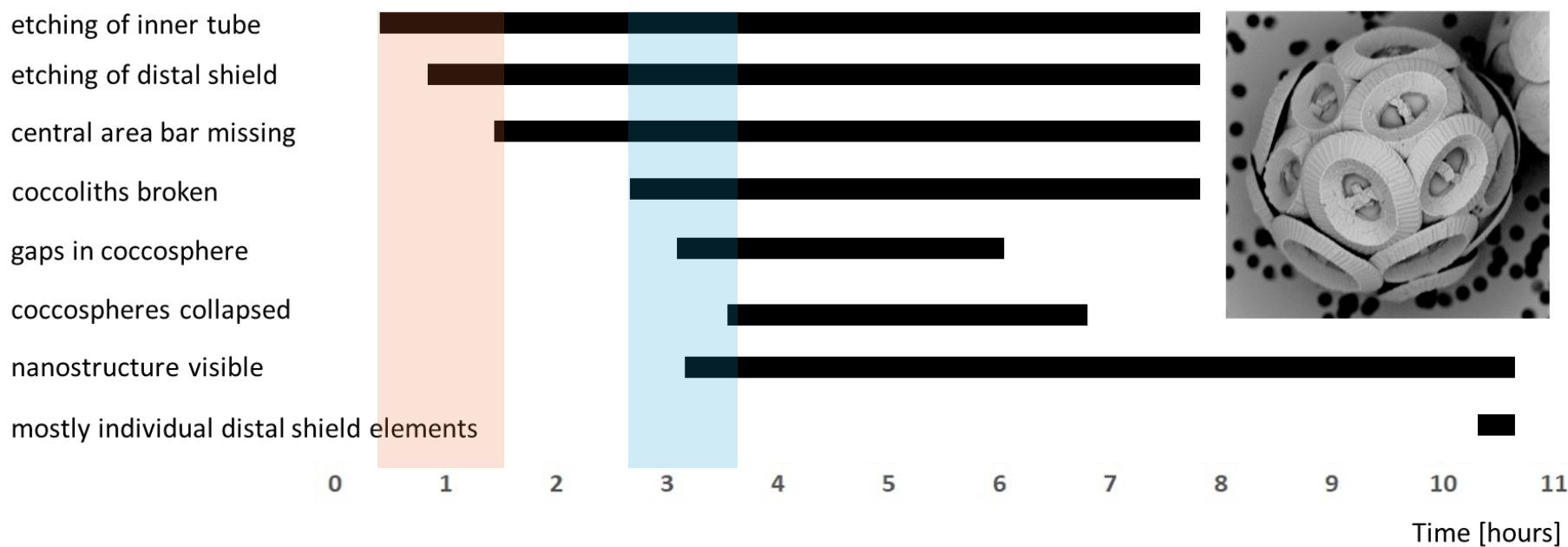


Fig 5 *Scyphosphaera apsteinii*

A) coccosphere at t0, no dissolution B) lopadolith base etching (be);
murolith centre missing (cm) C) lopadolith barrel etching (re) and
serrated rim (sr) D and E) broken lopadoliths F) isolated V-units G)
murolith at t0, no dissolution H) murolith with etching (me) I)
lopadolith in distal view showing R- and V-units (R- and V arrows,
Young 2008); and broken murolith (bm). All scale bars 5 μ m.

Fig 6

Coccolithus braarudii



Helicosphaera carteri



Scyphosphaera apsteinii

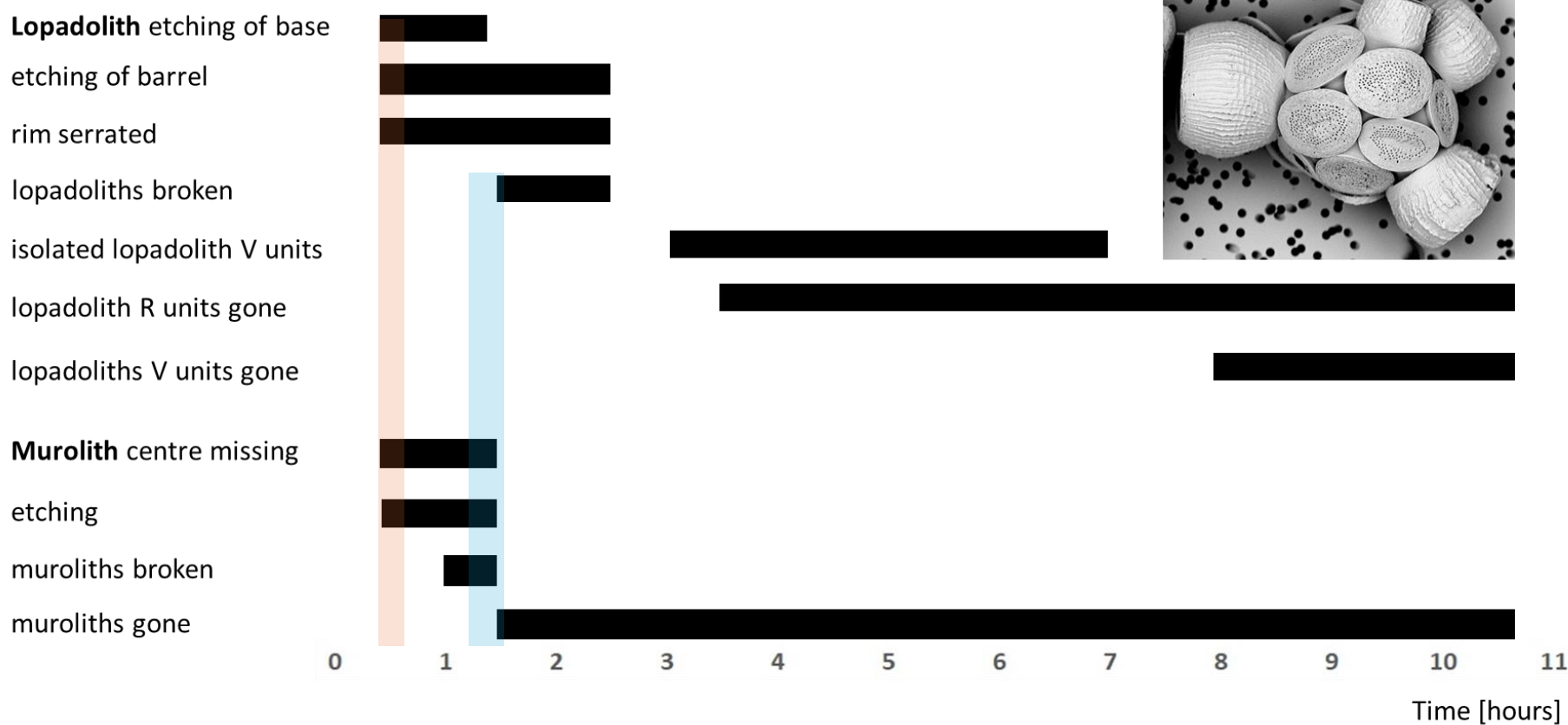


Fig 6 Timelines of dissolution. Bars indicate the period during which the respective feature can be observed. Shaded backgrounds indicate the onset points of major features. Pink backgrounds indicate the onset of etching, blue backgrounds indicate the onset of breakage/collapse. For example-images of each feature see Figs 1-5.

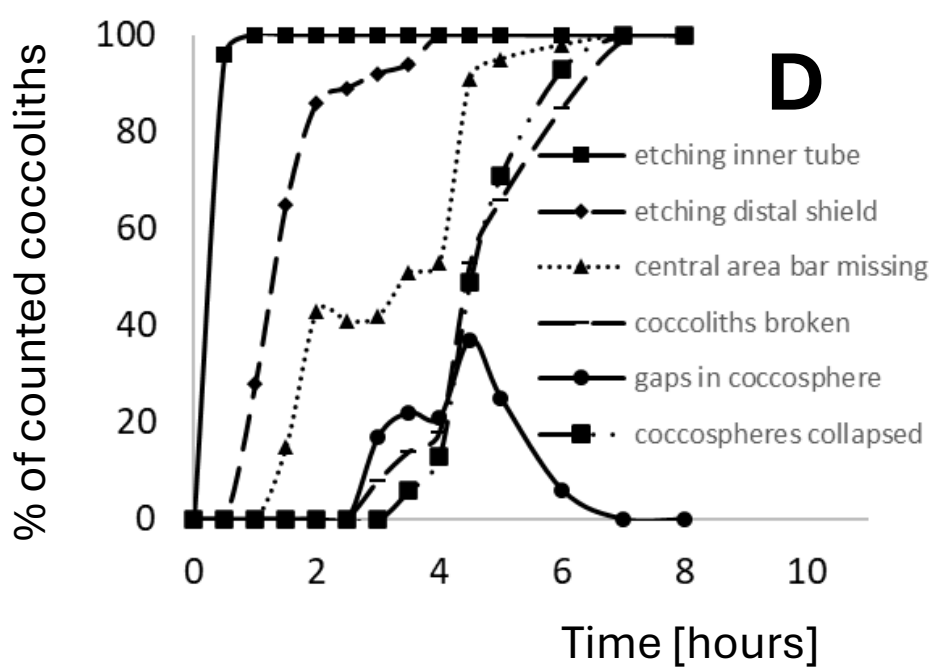
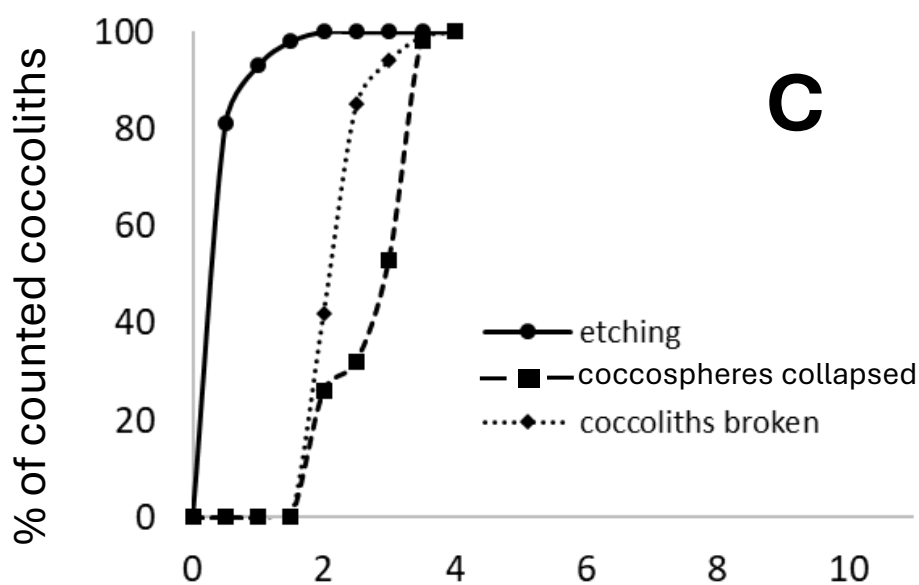
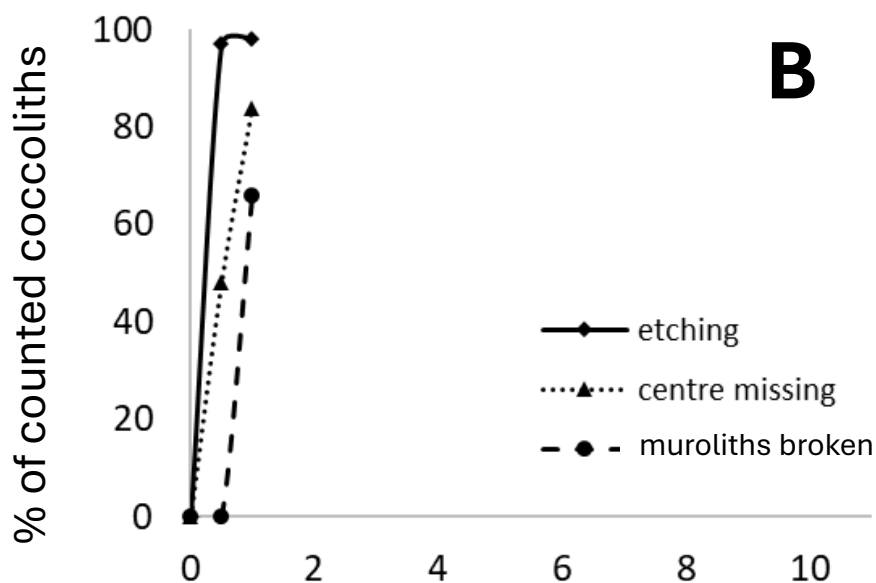
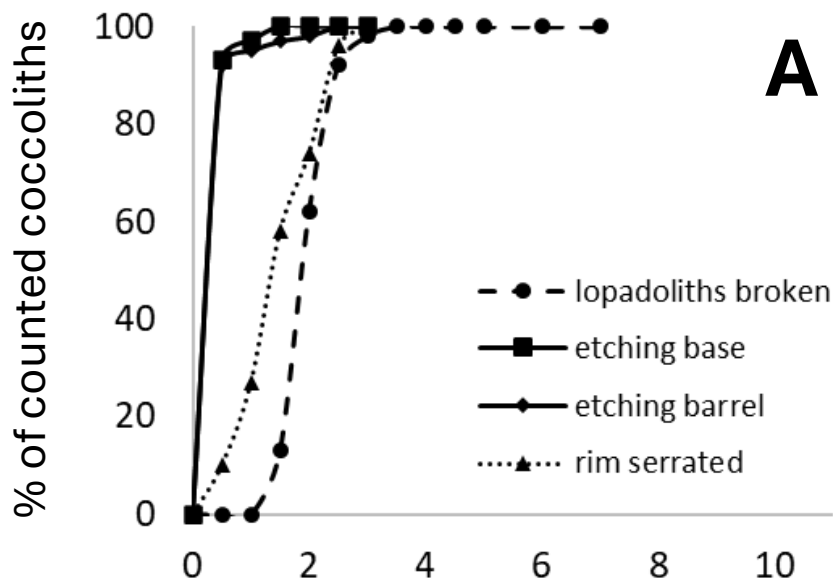


Fig 7 Quantification of the observations illustrated in Fig 6. Plotted is the percentage of each analysed feature versus time in hours from start of experiment. A) *Scyphosphaera apsteinii* lopadoliths B) *Scyphosphaera apsteinii* muraliths C) *Helicosphaera carteri* D) *Coccolithus braarudii*

Fig 8

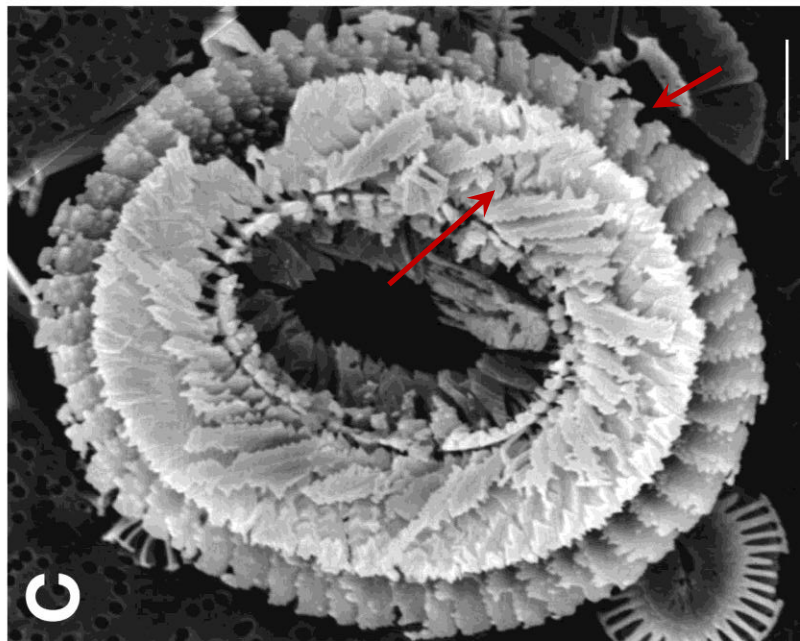
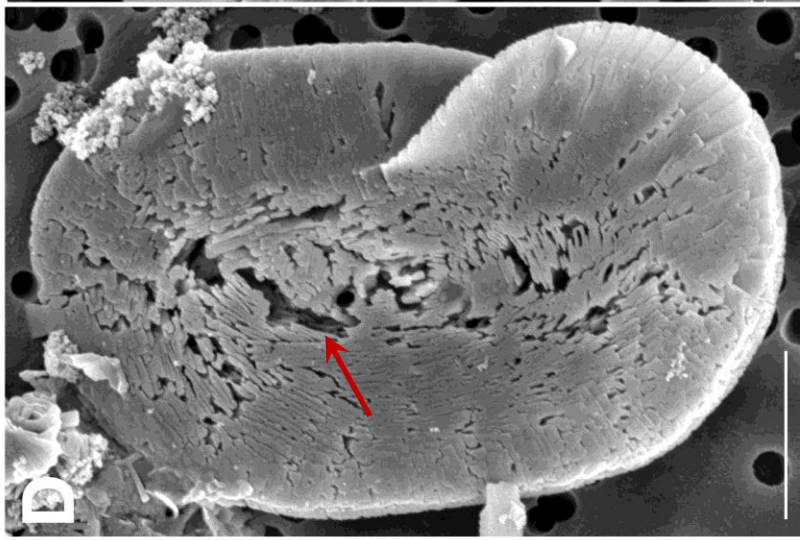
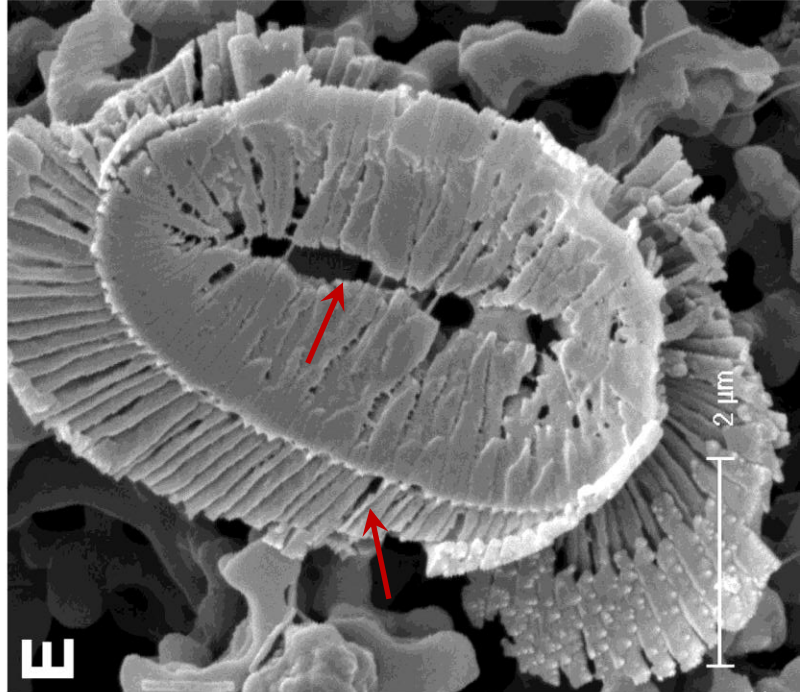


Fig 8 Field samples showing etching patterns comparable to those seen in the experimental samples (arrows). All scale bars 2 μm .

Coccolithus braarudii: A) Lower surface of a broken piece of distal shield showing nanostructure. B) Central area of distal shield showing early stage dissolution. C) Proximal surface showing advanced dissolution.

Helicosphaera carteri: D) Distal Surface showing early stage dissolution. E) Proximal surface showing advanced dissolution.

A, B - sediment trap samples from 3200m, N. Atlantic; C - surface water sample, NW Atlantic; D- sediment trap sample, Canaries, 200m; E plankton sample from 120m, Gulf of Mexico.